PAPER

Thermophoretic particle deposition effect on a squeezed flow of radiative Jeffrey fluid past a sensor surface with uniform heat source/sink and chemical reaction

To cite this article: Sajeel Mazhar *et al* 2024 *Phys. Scr.* 99 125966

View the article online for updates and enhancements.

IOP Publishing Phys. Scr. 99 (2024) 125966 https://doi.org/10.1088/1402-4896/ad906a

Physica Scripta

PAPER

CrossMark

RECEIVED
29 August 2024

REVISED
17 October 2024

ACCEPTED FOR PUBLICATION
8 November 2024

PUBLISHED
25 November 2024

Thermophoretic particle deposition effect on a squeezed flow of radiative Jeffrey fluid past a sensor surface with uniform heat source/sink and chemical reaction

Sajeel Mazhar[1], **Muhammad Ramzan**[1], **Ahmed S Sowayan**[2], **C Ahamed Saleel**[3,4], **Abdulkafi Mohammed Saeed**[5], **Seifedine Kadry**[6,7] **and Mohammed A El-Meligy**[8,9]

[1] Department of Computer Science, Bahria University, Islamabad, 44000, Pakistan
[2] Mechanical Engineering, College of Engineering, Al Imam Mohammad Ibn Saud Islamic University (IMSIU) Riyadh, Saudi Arabia
[3] Central Labs, King Khalid University, AlQura'a, Abha, PO Box 960, Saudi Arabia
[4] Department of Mechanical Engineering, College of Engineering, King Khalid University, PO Box 394, Abha 61421, Saudi Arabia
[5] Department of Mathematics, College of Science, Qassim University, Buraydah 51452, Saudi Arabia
[6] Department of Computer Science and Mathematics, Lebanese American University, Beirut, Lebanon
[7] Department of applied data science, Noroff University College, Norway
[8] Jadara University Research Center, Jadara University, Jordan
[9] Applied Science Research Center, Applied Science Private University, Amman, Jordan

E-mail: mramzan@bahria.edu.pk

Keywords: thermophoretic particle deposition, sensor surface, squeezed jeffrey fluid flow, thermal radiation

Abstract

This anticipated model investigates the time-dependent, and incompressible 2D magnetized Jeffrey liquid flowing on a sensor surface placed between two infinite parallel plates with the existence of a uniform heat source/sink. The lower plate remains fixed while the upper plate is subject to squeezing. For the heat and mass transmission processes, the consequences of radiative heat flux, chemical reaction, and thermophoretic particle deposition are applied and analyzed. The envisioned model is supported by prescribed heat and mass flux conditions. The uniqueness of the proposed model is the analysis of the unsteady squeezed flow of Jeffrey liquid over a sensor surface, accounting for radiative heat flux, thermophoretic particle deposition, and variable thermal conductivity. The model possesses applications in microfluidic sensors, biomedical devices, thermal management systems, and inkjet printing. The equations comprising the model are subject to similarity transformations. The bvp4c package is utilized to analyze the dynamic flow system. The connotation of arising parameters with the associated profiles is depicted through graphs and tables. It is examined that fluid velocity, temperature, and concentration profiles are dwindling functions of squeezed parameter. It is also witnessed that the concentration of liquid drops with an enhancement of thermophoretic and chemical reaction parameters. The validation of the truthfulness of the envisioned model is an added feature of this study.

Nomenclature

Symbols	Description
u, v	Components of velocity $[m/s]$
P	Pressure $[\mathrm{Kg}/ms^2]$
T	Liquid temperature [K]
B_0	Magnetic induction [T]
$k(T) = k_0[1 + \varepsilon\theta]$	Temperature-dependent thermal conductivity
Q_0	Volumetric rate of heat generation/absorption $[\mathrm{Kg}/ms^3\mathrm{K}]$
K_0	Rate of chemical reaction

C_p	Specific heat capacity [JKg/K]
U	External free stream velocity [m/s]
C	Concentration [mol/m^3]
a	Strength of squeezed flow
k^*	Mean absorption coefficient
b	Squeezing flow parameter
D_m	Molecular diffusivity [m^2/s]
k_0	Thermal conductivity [W/mK]
k^o	Thermophoretic coefficient
T_∞	Free stream temperature
C_∞	Concentration at the upper plate
Greek Symbols	
λ_1	Relaxation time
ν	Kinematic viscosity [m^2/s]
σ	Electrical conductivity [S/m]
η	Similarity variable
α	Thermal diffusivity [m^2/s]
λ	Relaxation to retardation ratio
σ^*	Stefan–Boltzmann constant [W/m^2K^4]
ε	Variable thermal conductivity parameter
ρ	Fluid density [kg/m^3]

Introduction

Non-Newtonian liquids are of interest to a lot of researchers because of their fascinating properties and practical significance in medical, and engineering applications, including polymer processing, blood flow in the circulatory system, magma, food mixing, multi-grade oils, and food mixing, among others. Non-Newtonian liquid mechanics theory is important to predict the behaviors of high molecular weight fluids [1–4], as Newtonian liquids are insufficient for this purpose. Furthermore, a solitary mathematical model is inadequate to encompass all of the rheological fluid characteristics of non-Newtonian liquids because of the flow diversity. The literature contains a wide range of fluid models that address various fluid aspects, one of which is the Jeffrey model. This linear model is simpler than other non-Newtonian fluid models, as it uses time derivatives instead of convective derivatives. There are a few studies that have concentrated on examining the flow of Jeffrey liquid by applying various constraints. Nadeem *et al* [5] scrutinized Jeffrey liquid flow over an exponentially stretched surface. MHD boundary layer flow and thermal transmission of a Jeffrey liquid across an extended sheet are examined by Ahmad and Ishak [6] with the effect of frictional heating. Turkyilmazoglu and Pop [7] obtained an analytical solution of the flow to the stagnation point in a Jeffrey liquid flow due to a stretching/shrinking surface. Qasim [8] worked using a stretched sheet under the influences of heat and mass transmission and studied the Jeffrey liquid flow by considering the heat source/sink. Bhatti *et al* [9] computed the MHD flow of the Jeffrey model on peristaltic blood within porous media. Kothandapani and Srinivas [10] examined the peristaltic features of a Jeffrey liquid model in an asymmetric geometry. A numerical model is computed by Narayana and Babu [11] in which Jeffrey fluid is analyzed over a stretched sheet with chemical reactions. Hayat and Mustafa [12] worked with time-dependent mixed convection Jeffrey liquid flow passing via porous vertically stretched surface under the effect of radiative flux. Ramesh and Joshi [13] found the numerical solutions for the flow of Jeffrey liquid along a porous medium within two parallel plates, by considering three fundamental unsteady flows. Moreover, Nadeem *et al* [14, 15] conducted mathematical studies on the peristaltic flow of Jeffrey liquids.

Squeezing flow involves polymer manufacturing, suction/injection operations, hydro-mechanical machinery, and the movement of synthetics inside living beings. Due to practical applications in industrial processes and some other fields such as injection molding, biophysical, chemical engineering, physical, polymer processing, and food engineering, the research on squeeze flow has attained importance in research fields. Initially, Stefan [16] put efforts into describing mathematical modeling for the viscous fluid squeezed flow across two parallel plates using an increasing degree of external squeezing phenomenon. Also, by using the Hermitian finite difference technique, Bhattacharyya and Pal [17] studied the electromagnetic unsteady squeezed flow in a channel consisting of two parallel discs in which the lower disc was revolving, with a result that the torque over the revolving disc is magnified as the Lorentz force increases. Recent research has also focused on non-Newtonian magnetic squeezing flows. Khan *et al* [18] performed the squeezed flow of Casson liquid influenced by magnetohydrodynamic effects, traversing in a spongy media. With the repercussion of a transverse magnetic flux squeezed flow of Carreau-Yasuda liquid due to a horizontal surface is investigated by Salahuddin *et al* [19]. However, some significant research on heat transfer mechanisms in squeezing flows with magnetized sensors has also been revealed. In this regard, the work of Shankar and Naduvinamani [20] who observed the simulations of the MHD squeezing flow of an unsteady Prandtl-Eyring liquid in a parallel plate sensor design and came up with results that elevating the magnetic parameter causes the lubricant to cool and flow more quickly, also by decreasing temperature magnitudes was possible with a larger plate permeability velocity value, is of significance importance. Khan *et al* [21] analyzed Carreau liquid squeezed flow due to a sensor geometry located with temperature dependent thermal conductance and came up with results that both velocity and temperature profiles enhance as the squeezed flow parameter escalates. Muhammad *et al* [22] scrutinized the unsteady, Jeffrey liquid flow in a squeezed channel having a stretched lower wall which was considered permeable.

Materials exhibiting variable thermal conductivity find diverse applications across engineering, energy storage, and other scientific domains, contributing to improved efficiency and performance, therefore the concept of temperature-dependent thermal conductivity has gained the attention of researchers. Muhammad *et al* [23] comprehended the role of unsteady flow of non-Newtonian liquid through a squeezed regime of parallel plates consisting of a micro-cantilever sensor. Alharbi *et al* [24] summarized the squeezing Casson nanofluid flow with variable thermal conductivity and viscosity. Furthermore, Atif *et al* [25] worked with sensor surface taking time-dependent Carreau fluid by considering the effect of radiative flux and varying thermal conductivity within a squeezed conduit. The flow of tangent hyperbolic liquid with temperature-dependent thermal conductivity over a sensor surface located within a squeezed channel was explored by Kumar *et al* [26], with the observation that there is a decline in velocity profile due to enhancement in the squeezed flow index parameter. Hamad *et al* [27] determined the response of thermal jump constraint on the flow of Jeffrey liquid across a stretching/shrinking sheet while accounting for varying thermal conductivity.

Many scholars are currently intrigued by the role of heat source and sink on liquid flow problems because of their ability to control heat exchange. In a recent study by Ramesh *et al* [28], an examination of thermal distribution was conducted by applying the effect of thermal source/sink in channels that were convergent/divergent and found that increasing the thermal source/sink parameter enhances thermal distribution. The consequences of the thermal source/sink on the thermal distribution is computed by Madhukesh *et al* [29]. By taking into consideration of thermal source/sink and radiative flux Khan and Hamid [30] conducted the performance of 2D flow of Williamson liquid, the research indicates that thermal performance improves with sink to source.

The phenomenon of thermophoretic particle deposition has attracted significant attention due to its practical applications, particularly in the field of engineering which includes building powdered coal burners, air cleaners, nuclear reactor protection, ventilation systems, and thermal exchangers. Goren [31] put a pioneering effort into the study of thermophoretic particle deposition. The work on the impacts of Thermophoretic particle deposition with different geometries is listed in [32–34]. Considering the effect of thermophoretic particle deposition the of Casson liquid flow which was dual stratified having magnetic dipole is explored by Chen *et al* [35]. The flow of a variable viscous ferromagnetic liquid along an extended cylinder, considering the influence of a thermal source/sink, and later, Casson liquid flow due to a horizontal thin needle, and Maxwell liquid flow over a stretched geomtery, considering the term of thermophoretic particle deposition were computed by Kumar *et al* [36–38].

From the research work mentioned above it is noticed that the unsteady squeezed flow of Jeffrey liquid over a sensor geometry under the consequences of radiative heat flux and thermophoretic particle deposition considering variable thermal conductivity is not yet discussed. The viscoelastic properties of Jeffrey fluid make it a key component in fluid mechanics and blood flow studies. The implementation of radiative flux and thermophoretic particle deposition in practical applications and the important role of thermal source/sink, variable thermal conductivity, and chemical reaction in research and engineering fields, motivates the present study to analyze the impact of all these effects on Jeffrey fluid. The considered geometry is a flow along a permeable sensor geometry located within a squeezed channel. None of the above cited and even existing literature simultaneously analyzed such effects. The resulting mathematical model is made up of nonlinear PDEs that, after undergoing the proper mathematical transformations, are transformed into nonlinear ODEs that can be solved numerically employing bvp4c. The uniqueness of the anticipated model is displayed in table 1 by making a comparison with closely published works.

Mathematical formulation

The two-dimensional, laminar, and unsteady squeezing flow of Jeffrey liquid through a microcantilever sensor surface is analyzed. S depicts the extra stress tensor for the Jeffrey liquid is described as under [39]:

$$S = \frac{\mu}{1+\lambda}\left(A_1 + \lambda_1 \frac{dA_1}{dt}\right), \tag{1}$$

where $A_1 = (grad\ V) + (grad\ V)^T$, indicates first Rivlin Ericksen tensor.

The following are the presumptions:

- The flow is represented using the xy-coordinate system, where the y-axis is positioned perpendicular to the flow surface and x-axis points along the direction of the flow.
- Flow is due to the free stream velocity U and a constant magnetic flux of intensity B_0 implemented normal to the surface.
- The squeezing channel consists of two infinite horizontal parallel plates and a permeable sensor of length L which is placed horizontally between these plates.
- The channel has a time-dependent height $h(t)$, which is significantly larger than the thickness of boundary layer.
- The lower plate stays stationary while the upper plate is compressed.
- It is assumed that the thermal conductance of liquid varies with temperature.
- During fluid heat transport, the consequences of radiative heat flux and heat generation are taken into account.
- A first-order chemical reaction and thermophoretic particle deposition are assumed to exist for mass transfer.
- The geometry of the assumed flow model is given in figure 1.

The system of equations is developed as under [12, 40–43]:

Equation of continuity

$$u_x + v_y = 0, \tag{2}$$

Momentum equation

$$u_t + uu_x + vu_y = -\frac{1}{\rho}P_x + \frac{\nu}{1+\lambda}[u_{yy} + \lambda_1(u_{yyt} + uu_{yyx} + vu_{yyy} - u_x u_{yy} + u_y u_{yx})] - \frac{\sigma B_0^2}{\rho}u, \tag{3}$$

where ν indicates the viscosity parameter, λ represents the ratio of relaxation and retardation times, and λ_1 indicates the relaxation time. The strength of the magnetic field is represented by B_0.

Free stream equation

$$U_t + UU_x = -\frac{1}{\rho}P_x - \frac{\sigma B_0^2}{\rho}U. \tag{4}$$

When the pressure gradient is excluded using equations (2) and (3), the resulting momentum conservation equation will be

$$u_t + uu_x + vu_y = U_t + UU_x + \frac{\nu}{1+\lambda}[u_{yy} + \lambda_1(u_{yyt} + uu_{yyx} + vu_{yyy} - u_x u_{yy} + u_y u_{yx})] + \frac{\sigma B_0^2}{\rho}[U - u], \tag{5}$$

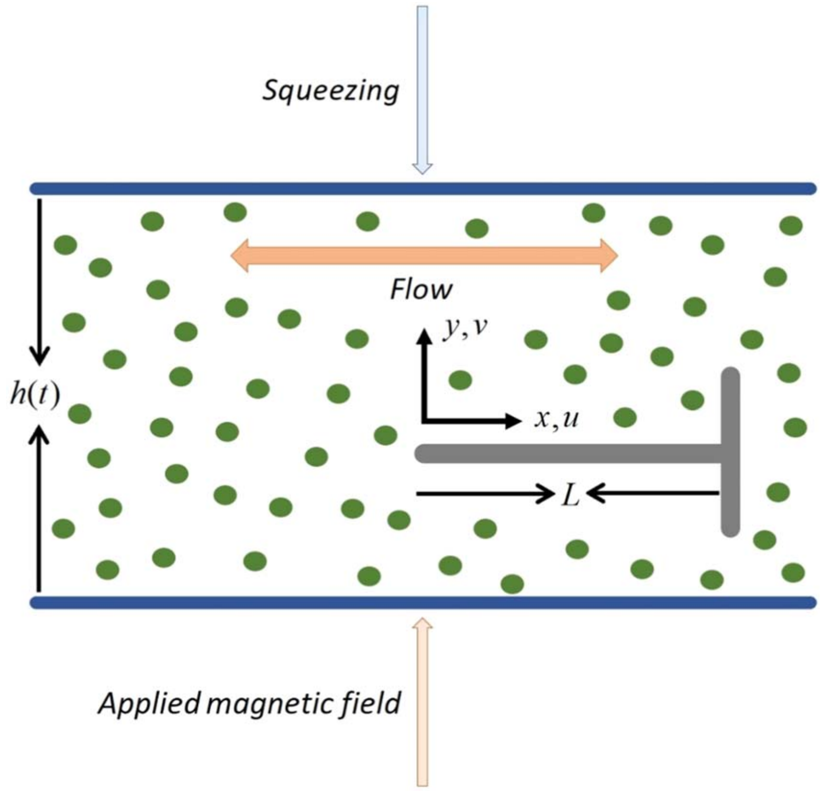

Figure 1. Geometry of assumed flow problem.

Temperature equation

$$T_t + uT_x + vT_y = \frac{1}{\rho C_p}[[k(T)T_y]_y - [q_r]_y] + \frac{Q_0}{\rho C_p}(T - T_\infty), \tag{6}$$

where $k(T)$ is the variable thermal conductance and Q_0 represents the heat source/sink term with $Q_0 > 0$, is the for the source term and $Q_0 < 0$, is for the sink term.

Concentration equation

$$C_t + uC_x + vC_y = D_m C_{yy} - K_0(C - C_\infty) - [U_T(C - C_\infty)]_y, \tag{7}$$

where the second last term in the above equation represents the 1st order chemical reaction and the last term signifies the thermophoretic term.

The term q_r in equation (6) is called radiative heat flux which is:

$$q_r = -\frac{4\sigma^*}{3k^*}[T^4]_y, \tag{8}$$

with $T^4 \cong 4T_\infty^3 T - 3T_\infty^4$, substituting it in equation (7) we obtain:

$$q_r = -\frac{16\sigma^*}{3k^*}T_\infty^3 T_y, \tag{9}$$

The term U_T in equation (7) is called thermophoretic velocity and is given as:

$$U_T = -\frac{k^o\nu}{T_r}T_y, \tag{10}$$

Associated constraints

$$u(x, 0, t) = 0, \; v(x, 0, t) = v_0(t),$$

$$-k_0[T(x, 0, t)]_y = q(x), \; -D_m[C(x, 0, t)]_y = h(x),$$

$$u(x, \infty, t) = U(x, t), [u(x, \infty, t)]_y = 0, T(x, \infty, t) = T_\infty, C(x, \infty, t) = C_\infty, \tag{11}$$

where $v_0(t) = v_r\sqrt{a}$ indicates the characteristic reference velocity on the sensor surface, $q(x) = q_0x$ represents the heat flux, and $h(x) = h_0x$ represents the mass flux.

Similarity transformations

$$U = ax, \psi = x\sqrt{a\nu}f(\eta), a = (s + bt)^{-1}, \eta = y\sqrt{\frac{a}{\nu}},$$

$$\eta = y\sqrt{\frac{a}{\nu}},$$

$$u = axf'(\eta), \theta(\eta) = \frac{T - T_\infty}{\frac{q_0x}{k_0}\sqrt{\frac{\nu}{a}}}, v = -f(\eta)\sqrt{a\nu}, \phi(\eta) = \frac{C - C_\infty}{\frac{h_0x}{D_m}\sqrt{\frac{\nu}{a}}}. \tag{12}$$

Using equation (12) into equations (5)–(7) we get

$$f''' + \delta_m\left((f'')^2 - 2bf''' - \left(f + \frac{b\eta}{2}\right)f^{iv}\right) + (1 + \lambda)\begin{bmatrix} 1 + \left(f + \frac{b\eta}{2}\right)f'' - (f')^2 \\ +M(1 - f') + b(f' - 1) \end{bmatrix} = 0, \tag{13}$$

$$(1 + \varepsilon\theta + R)\theta'' + \varepsilon(\theta')^2 - \Pr\left(f' + \frac{b}{2}\right)\theta + \Pr\left(f + \frac{b\eta}{2}\right)\theta' + \Pr Q\theta = 0, \tag{14}$$

$$\phi'' - Sc\gamma\phi - \tau Sc(\phi\theta'' + \theta'\phi') + Sc\left[\left(f + \frac{b\eta}{2}\right)\phi' - \left(f' + \frac{b}{2}\right)\phi\right] = 0, \tag{15}$$

and the associated transformed boundary conditions are obtained by substituting equation (12) into equation (11)

$$f'(0) = 0, f(0) = -f_0, \theta'(0) = -1, \phi'(0) = -1,$$
$$f'(\infty) \to 1, f''(\infty) \to 0, \theta(\infty) \to 0, \phi(\infty) \to 0, \tag{16}$$

where $\delta_m = a\lambda_1$ indicates Deborah number, $M = \frac{\sigma B_0^2}{\rho a}$ is the magnetic parameter, $R = \frac{16\sigma^* T_\infty^3}{3k^* k_0}$ indicates the radiation parameter, $\Pr = \frac{\nu}{\alpha}$ is Prandtl number, $Q = \frac{Q_0}{(\rho C_p)a}$ indicates heat generation/absorption coefficient, $Sc = \frac{\nu}{D_m}$ indicates the Schmidt number, $\gamma = \frac{K_0}{a}$ represents the chemical reaction factor, $\tau = -\frac{k^o q_0 x}{k_0 T_r}\sqrt{\frac{\nu}{a}}$ is the thermophoretic parameter.

The wall drag coefficient has a mathematical form:

$$Cf_x = \frac{2}{\rho_f U^2}\tau_w, \tag{17}$$

where τ_w is wall shear stress defined as

$$\tau_w = \frac{\mu}{1 + \lambda}[u_y + \lambda_1(u_{yt} + uu_{xy} + vu_{yy})]_{y=0}. \tag{18}$$

The dimensionless form of the wall drag coefficient is as follows:

$$\frac{1}{2}\sqrt{\mathrm{Re}_x}\,Cf_x = (1 + \lambda)^{-1}\left[f'' + \delta_m\left(\left(f' - \frac{3}{2}b\right)f'' - f'''f\right)\right]_{\eta=0}. \tag{19}$$

The local heat transmission rate has the mathematical form [44]:

$$Nu_x = \frac{x}{q_0x\sqrt{\frac{\nu}{a}}}q_w, \tag{20}$$

where q_w is wall heat flux is

$$q_w = q_r + \frac{\frac{q_0x}{k_0}k(T)}{\theta(\eta)}. \tag{21}$$

Dimensionless form of local heat transmission rate is as follows:

$$\frac{1}{\sqrt{\mathrm{Re}_x}}Nu_x = \left[\frac{1}{\theta(\eta)}(1+\varepsilon\theta(\eta)) - R\theta'(\eta)\right]_{\eta=0}. \tag{22}$$

The local mass flux has the mathematical form

$$Sh_x = \frac{x}{h_0 x\sqrt{\frac{\nu}{a}}}h_m, \tag{23}$$

where h_m is wall mass flux defined as

$$h_m = \frac{h_0 x}{\phi(\eta)}. \tag{24}$$

Dimensionless form of local mass flux is as follows:

$$\frac{1}{\sqrt{\mathrm{Re}_x}}Sh_x = \left[\frac{1}{\phi(\eta)}\right]_{\eta=0}. \tag{25}$$

In equations (19), (22), and (25) the parameter $\mathrm{Re}_x = \frac{ax^2}{\nu}$, represents the local Reynolds number.

Solution scheme

The above system is solved using a built-in bvp4c software in MATLAB with the 4th order accuracy and mesh size 0.01 with an error tolerance of 10^{-6}. The coupled, nonlinear ordinary differential equations expressed in equations (13)–(15) are converted into 1st order ODEs by applying the underneath approach:

$$\begin{aligned} &f = y_1,\, f' = y_2,\, f'' = y_3,\, f''' = y_4,\, f^{iv} = yy_1,\\ &\theta = y_5,\, \theta' = y_6,\, \theta'' = yy_2,\\ &\phi = y_7,\, \phi' = y_8,\, \phi'' = yy_3. \end{aligned} \tag{26}$$

With equation (26) the system of equations (13)–(15) with boundary conditions in equation (16) can be written as:

$$yy_1 = \frac{(1+\lambda)\left[1 + \left(y_1 + \frac{b\eta}{2}\right)y_3 - (y_2)^2 + M(1-y_2) + b(y_2-1)\right] + y_4 + \delta_m[(y_3)^2 - 2by_4]}{\delta_m\left(y_1 + \frac{b\eta}{2}\right)}, \tag{27}$$

$$yy_2 = \frac{\mathrm{Pr}\left[\left(y_2 + \frac{b}{2}\right)y_5 - \left(y_1 + \frac{b\eta}{2}\right)y_6 - Qy_5\right] - \varepsilon(y_6)^2}{(1+\varepsilon y_5 + R)}, \tag{28}$$

$$yy_3 = Sc\left[\gamma y_7 + \tau(y_7 yy_2 + y_6 y_8) - \left[\left(y_1 + \frac{b\eta}{2}\right)y_8 - \left(y_2 + \frac{b}{2}\right)y_7\right]\right], \tag{29}$$

with boundary conditions,

$$\begin{aligned} &y_2 = 0,\, y_1 = -f_0,\, y_6 = -1,\, y_8 = -1 \text{ at } \eta = 0\\ &y_2 \to 1,\, y_3 \to 0,\, y_5 \to 0,\, y_7 \to 0 \text{ as } \eta \to \infty \end{aligned} \tag{30}$$

A flow diagram of the implemented scheme bvp4c is added in figure 2.

Results and discussions

This section elucidates a discussion about the core outcome of the existing study. The influence of various important emerging parameters in the problem on their respective profiles is examined through graphs and discussed briefly. Furthermore, the role of λ and δ_m over the wall drag coefficient, b and Q on the heat transmission rate, τ and γ on the Sherwood number are presented through tables. The non-dimensional flow control physical parameters encountered in the problem with values assigned to them are given below:

$$\begin{aligned} &0.2 \leqslant b \leqslant 0.8,\, 0.1 \leqslant \lambda \leqslant 0.7,\, 0.5 \leqslant \delta_m \leqslant 0.7,\, 0.3 \leqslant Q \leqslant 0.6,\, R = 0.9,\, M = 0.2,\\ &\tau = 0.5,\, 0.5 \leqslant \gamma \leqslant 0.7,\, \mathrm{Pr} = 0.5,\, 0.5 \leqslant \eta \leqslant 1.7,\, f_0 = 0.3,\, \varepsilon = 0.5,\, Sc = 0.9. \end{aligned}$$

For convenience, this section is divided into the following subsections:

i. Interpretation of velocity profile versus varied parameters

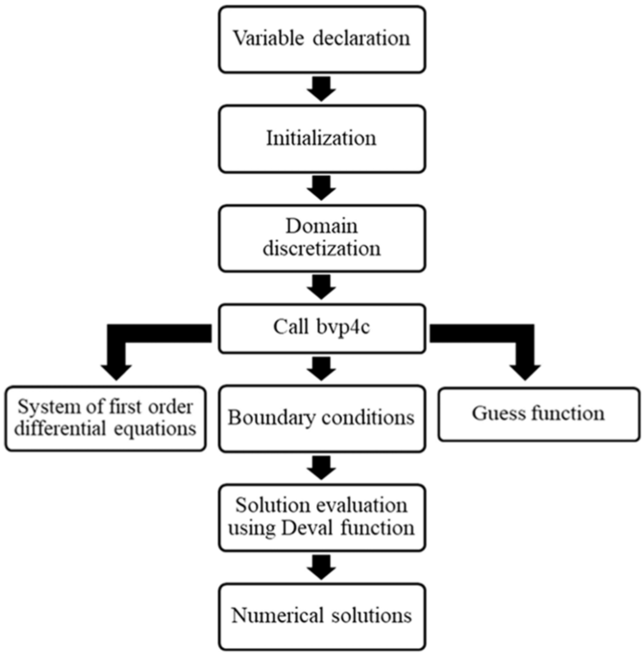

Figure 2. Flow chart of utilized numerical scheme.

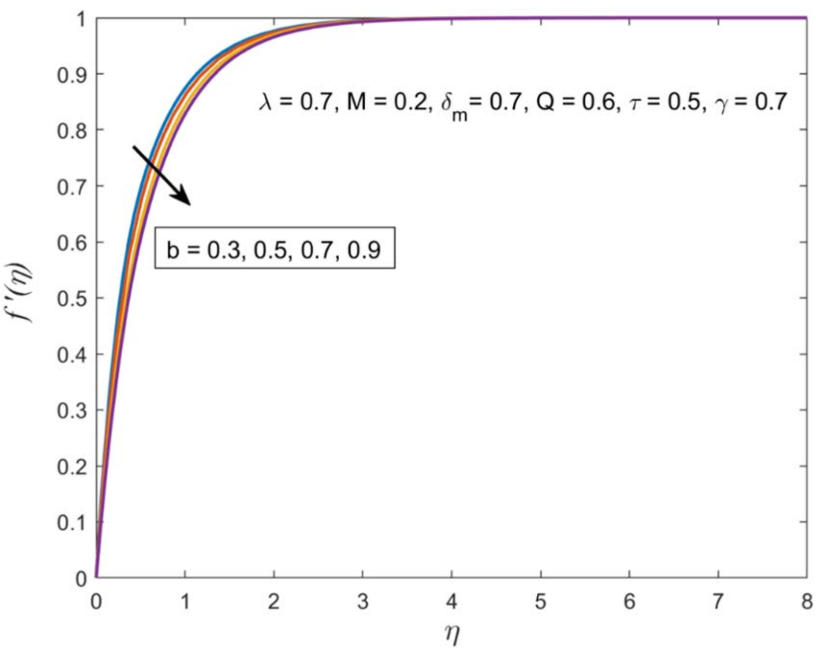

Figure 3. Illustration of $f'(\eta)$ with squeezed flow parameter.

ii. Interpretation of temperature profile versus varied parameters

iii. Interpretation of concentration profile versus varied parameters

iv. Tabular Discussion

Interpretation of velocity profile

Figure 3 clarifies that the velocity of liquid drops for elevating counts of squeezed flow factor. It happens due to the kinetic energy of liquid particles increases as the squeezing phenomenon intensifies. However, there exists an

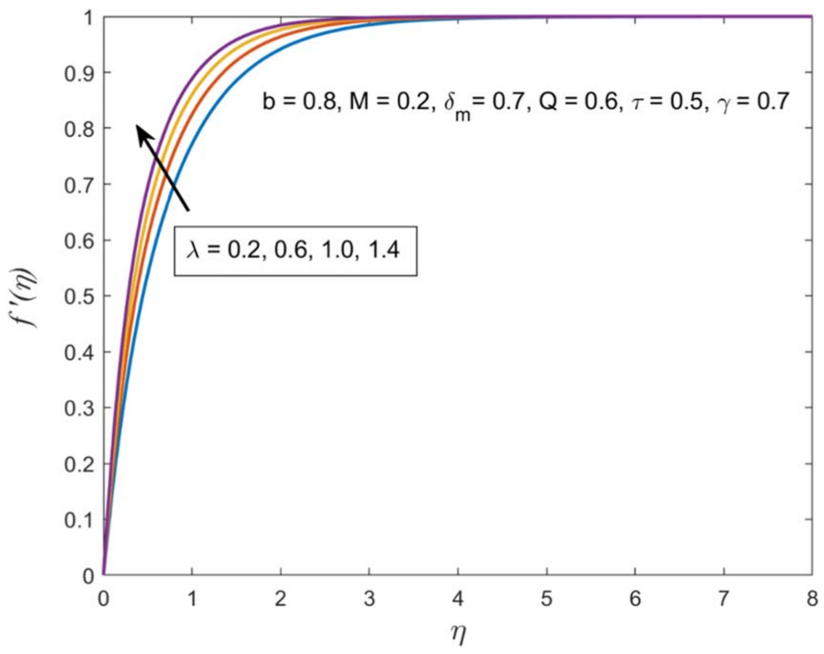

Figure 4. Illustration of $f'(\eta)$ with Jeffrey model parameter.

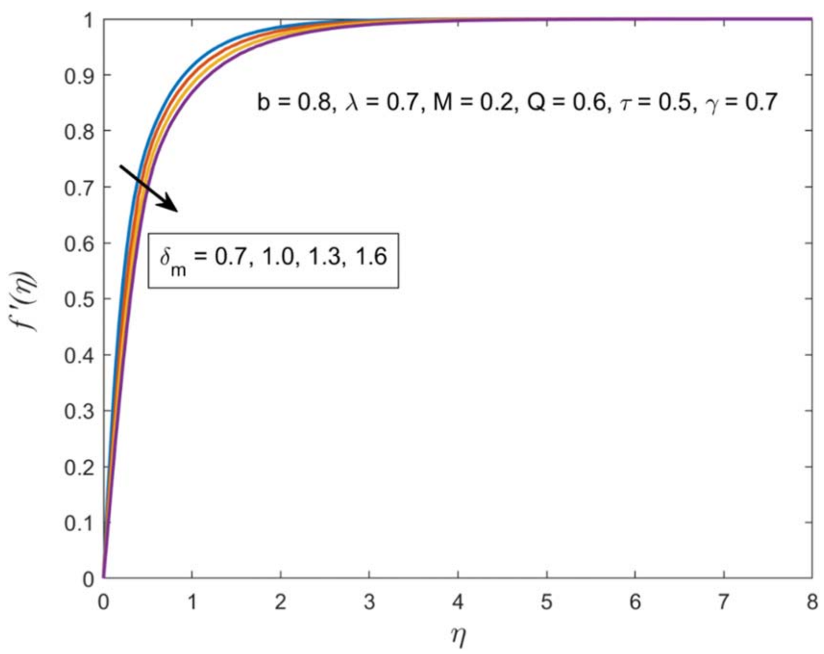

Figure 5. Illustration of $f'(\eta)$ with Deborah number.

inverse relation among the strength of the squeeze flow and the squeezing flow parameter. Consequently, this shows a reduction in the velocity distribution.

The role of the Jeffrey model parameter on the velocity profile is illustrated in figure 4. This plot clarifies that the velocity field is a growing function of the Jeffrey model factor. The velocity profile enhances for varied estimates of Jeffrey model parameter because relaxation and retardation times influence the flow of fluid under stress and reduce the fluid resistance to flow, eventually, the increased fluid velocity is visualized.

The association of fluid velocity with the Deborah number is depicted in figure 5. Here, the repercussion of the Deborah number is opposite to the effect of the Jeffrey model factor on the velocity profile means velocity of fluid is on the decline for the numerous estimations of Deborah number. This is because of the dominance of the elastic forces that change the fluid-like behavior to solid-like. This enhanced resistance to fluid flow results in lowering the fluid velocity.

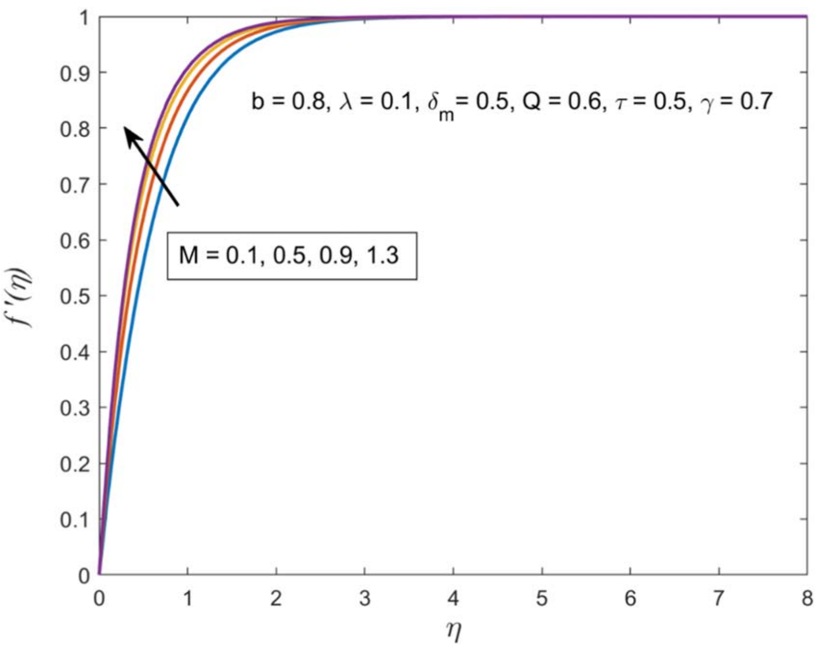

Figure 6. Illustration of $f'(\eta)$ with magnetic parameter.

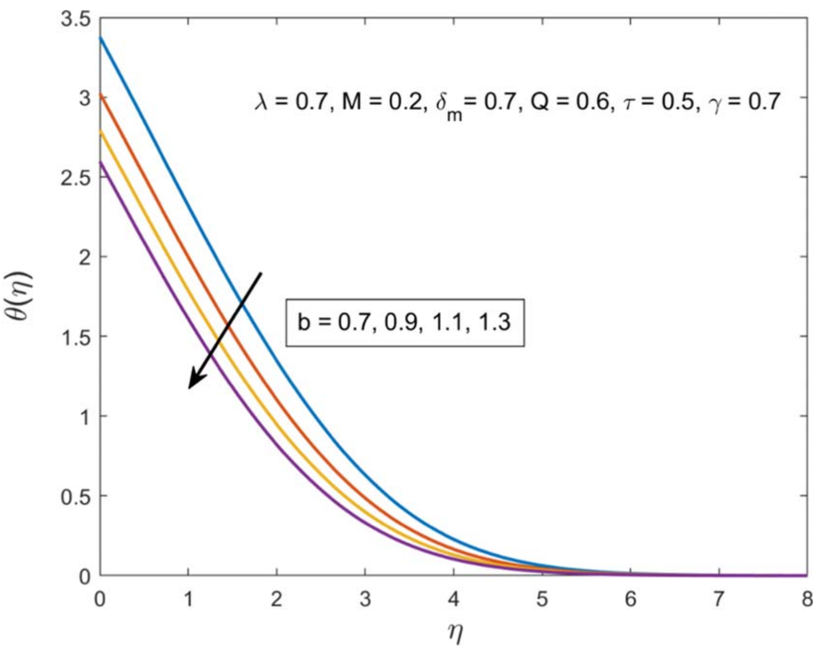

Figure 7. Illustration of $\theta(\eta)$ with squeezed flow parameter.

Figure 6 shows the rise in velocity profile for amplification in magnetic parameter. This occurs because when the value of M increases, resistance in the flow rises. However, the effect of M cancels due to the squeezing of an upper surface, and the fluid flow around the sensor wall increases, resulting in an elevation of the velocity distribution. As the MHD effect elevates the velocity profile, it means the magnetic field may accelerate or decelerate specific regions of the flow. This flexibility optimizes flow characteristics for various applications. Also, it improves model accuracy by aligning theoretical predictions with experimental results, which leads to a more accurate representation of physical systems like MHD pumps, generators, and electromagnetic brakes.

Interpretation of temperature profile

From figure 7 it can be noted that the temperature profile supresses for higher estimations of squeezed flow parameter. This happens because generally when the squeezed flow parameter increases, this results in a

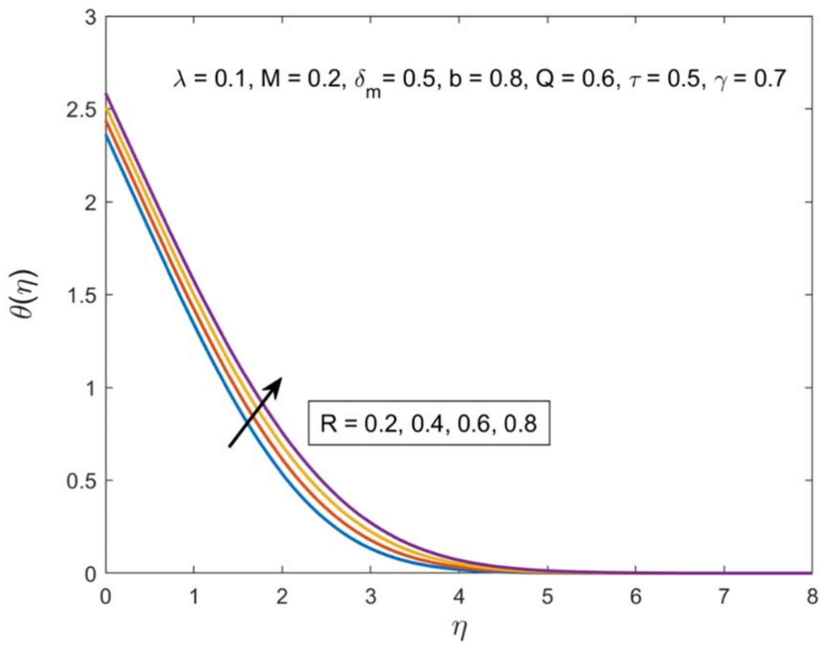

Figure 8. Illustration of $\theta(\eta)$ with radiation parameter.

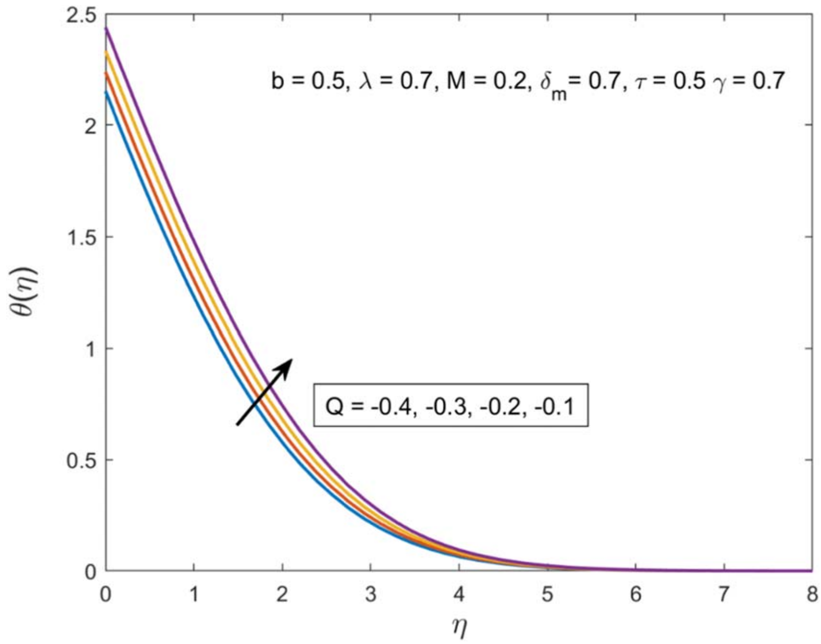

Figure 9. Illustration of $\theta(\eta)$ with heat absorption coefficient.

decrease in the kinetic energy of liquid particles which leads to a subsequent reduction in temperature. The radiation parameter is a dimensionless quantity that exhibits a ratio of heat transfer via thermal radiation to heat transmission via conduction. The role of the radiation factor on the temperature field is depicted in figure 8. According to this plot, there is an enhancement in the temperature profile with incremented values of the radiation parameter. Physically, for higher counts of radiation parameter radiation prevails over conduction, also mean absorption coefficient decays, and as a result temperature of the fluid upsurges.

Figures 9 and 10 point out that an upsurge in values of heat generation/absorption coefficient enhanced the temperature profile and relevant thickness. In fact, the coefficient of heat generation/absorption accelerates the heat transport phenomenon occurring on the surface and the absorption of heat causes a rise in the kinetic energy of liquid particles, leading to an enhancement in the temperature of the fluid.

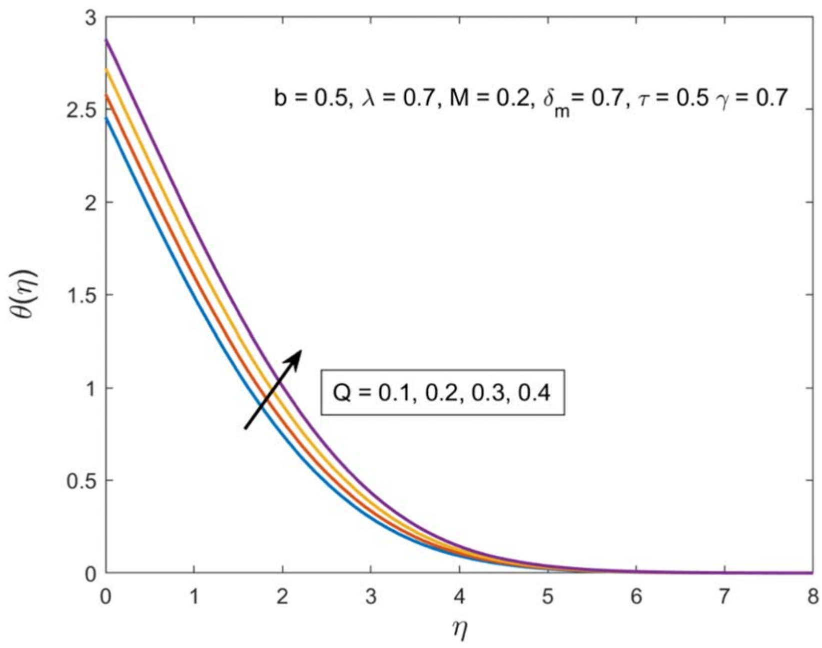

Figure 10. Illustration of $\theta(\eta)$ with heat generation coefficient.

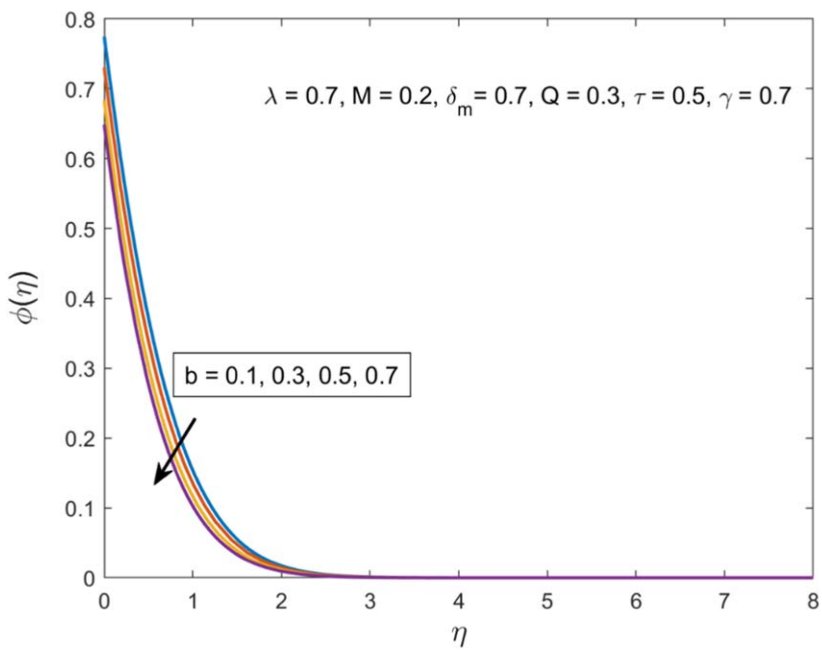

Figure 11. Illustration of $\phi(\eta)$ with squeezed flow parameter.

Interpretation of concentration profile

Figure 11 shows the trend of the concentration profile with the squeezed flow parameter. It is clear from this plot that enlarging the squeezed flow parameter decreases the concentration profile. Owing to squeezing, a stronger compression of the liquid between the plates is observed resulting in a high-pressure gradient in the liquid leading to enhanced fluid velocity near the surfaces.

Figure 12 clarifies that the concentration profile shows decreasing behavior with thermophoretic parameter. This happens because of the positive values of the thermophoresis variable and the increasing effect of thermophoretic force which results in the movement of fluid particles from warm to cold surface.

The behavior of the concentration profile against chemical reaction parameter is explained in figure 13. This plot clarifies that there is a drop in the concentration profile for elevating counts of chemical reaction parameter. This happens because for large estimates of chemical reaction parameter, the reaction rate is fostered and

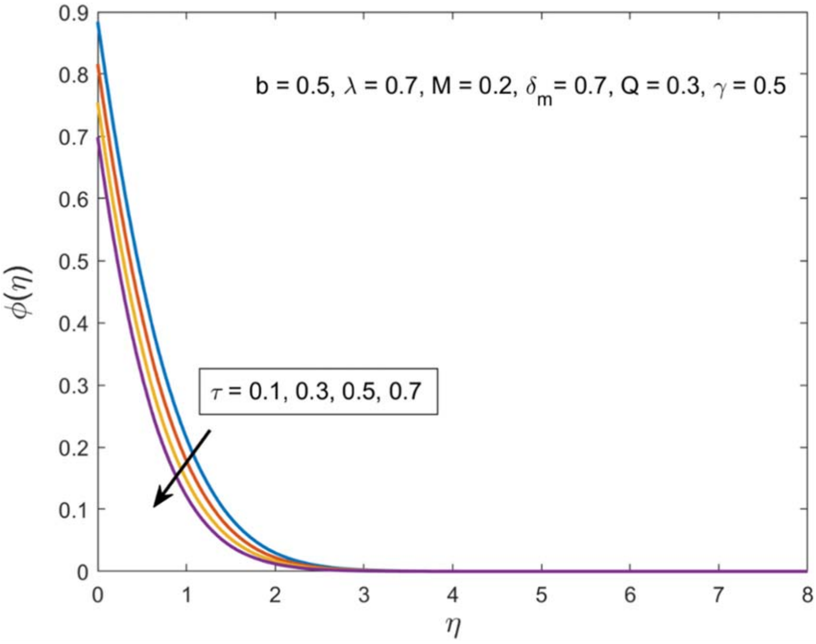

Figure 12. Illustration of $\phi(\eta)$ with thermophoretic parameter.

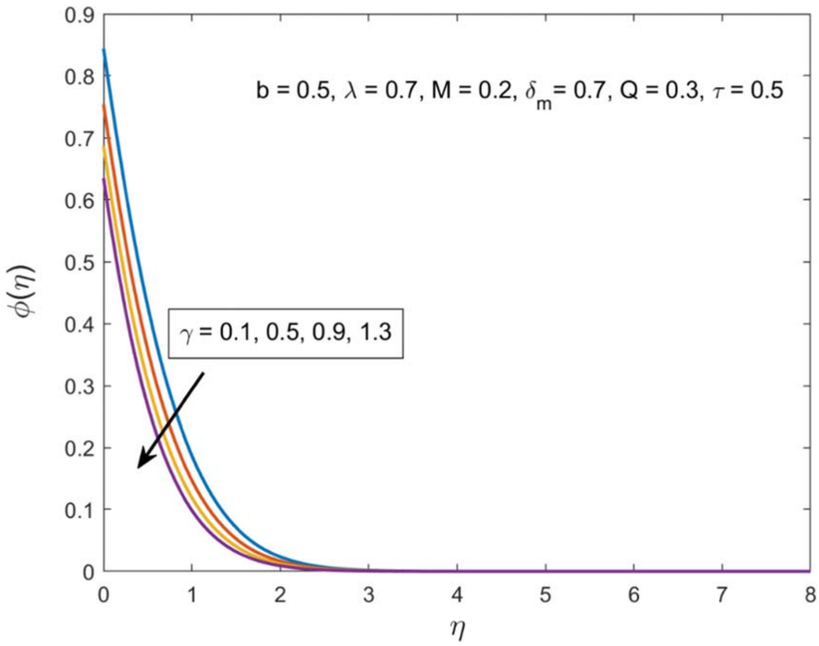

Figure 13. Illustration of $\phi(\eta)$ with chemical reaction parameter.

reactions are transmuted into products at a faster pace which results in a supression in the concentration of the reactants in the liquid leading to a declined concentration profile.

Tabular discussion

The behavior of friction factor with increment in Jeffrey fluid parameter λ and Deborah number δ_m is presented in table 2. According to the results, the wall drag coefficient exhibits increasing behavior for λ and decreasing for δ_m. The elastic behavior of fluid is influenced by Jeffrey fluid parameter. As Jeffrey fluid parameter is enhanced, the liquid depicts a solid-like behavior leading to more resistance to deformation. As a result, high shear stress at the surface is witnessed, and eventually, strong surface drag is spotted. In the second case, for high estimates of

Table 1. Originality of the present model.

Studies	Squeezed flow	Unsteady Jeffrey fluid flow	Temperature dependent thermal conductance	Heat source/sink	Radiative heat flux	Thermophoretic particle deposition
Hayat and Mustafa [12]	No	Yes	No	No	Yes	No
Atif *et al* [25]	Yes	No	Yes	No	Yes	No
Kumar *et al* [36]	No	No	No	Yes	No	Yes
Current	Yes	Yes	Yes	Yes	Yes	Yes

Table 2. Skin friction coefficient for Jeffrey model parameter and Deborah number.

λ	δ_m	Cf_x
0.2		−0.604668
0.6		−0.558168
1.0		−0.524970
1.4		−0.499018
	0.7	−0.723303
	1.0	−1.889510
	1.3	−3.093760
	1.6	−4.304650

Table 3. Nusselt number for squeezed flow parameter and heat generation coefficient.

b	Q	Nu_x
0.7		1.75414
0.9		1.78279
1.1		1.81429
1.3		1.84607
	0.1	1.82160
	0.2	1.80233
	0.3	1.78263
	0.4	1.76245

Table 4. Sherwood number for thermophoretic parameter and chemical reaction parameter.

τ	γ	Sh_x
0.1		1.20272
0.3		1.30024
0.5		1.40324
0.7		1.51153
	0.1	1.34865
	0.5	1.48728
	0.9	1.61455
	1.3	1.73271

the Deborah number, the relaxation time is much longer than the fluid flow time scale, and ultimately, the liquid flowing characteristic is compromised leading to the diminishing of shear forces. Thus, a drop in Surface drag is observed.

The performance of the local heat transmission rate with incrementing values of squeezed flow parameter b and heat generation coefficient Q is numerically presented in table 3. This table clarifies that the Nusselt number shows increasing and decreasing behaviors for b and Q respectively. Amplification of the squeezed flow parameter results in a higher liquid flow velocity near the surface; thus increasing the rate of heat transfer. In contrast, with an enhancement in the heat generation parameter values, the liquid produces more internal heat resulting in an overall rise in the fluid temperature. As the surface heat flux is fixed, the rate of heat transfer must drop to balance internal heat generation. That is why a declined heat transfer rate is observed.

Table 4 numerically explains the variation of the Sherwood number with increments in estimations of the thermophoretic parameter τ and chemical reaction parameter γ. According to outcomes, there is an enhancement in local mass flux for both τ and γ. Higher estimates of the thermophoretic parameter improve the particles' interaction thus increasing the fluid temperature and concentration gradient. Also, high chemical reaction parameter values indicate the faster consumption of reactants leading to a high concentration gradient.

Table 5. Validation of present results with published work of Rammoorthi and Mohanavel [45] by setting $\delta_m = \lambda = M = b = \varepsilon = R = \Pr = Q = Sc = \gamma = \tau = 0$, under different values of f_0 for $f''(0)$.

f_0	Rammoorthi and Mohanavel [45]	Present
1	0.756575206	0.756575207
0	1.232587780	1.232587781
−1	1.889314035	1.889314036

Table 5 illustrates a comparison of the present work with previous research. An excellent concurrence is obtained.

Concluding remarks

Two-dimensional, unsteady, magnetized squeezed flow of Jeffrey liquid with temperature-dependent thermal conductivity flow along a sensor surface under the role of chemical reaction, linear thermal radiation, thermophoretic particle deposition, and thermal source/sink is investigated. The proposed model has been supported by the prescribed heat and mass flux conditions. The bvp4c tool is utilized and the behavior of fluid under these effects has been analyzed through graphs to assort the flow-controlling backdrops, the impacts of some dimensionless numbers have been shown in tabular form.

This study owing to its interesting applications in daily life makes it unique from the earlier published works. It provides important insights into the behavior of Jeffrey fluids in squeezed flow conditions, which are applicable to a variety of industrial and biomedical systems. The viscoelastic properties, especially relaxation time, affect velocity and temperature profiles, enabling improved material control in polymer manufacturing, while in biomedical applications like artificial heart pumps, understanding the fluid's behavior can enhance the efficiency and longevity of fluid-handling devices. Further research into complex flow conditions could expand these applications across various industries.

Below is a list of some of the main conclusions:

- Velocity, and concentration distributions are dwindling functions of squeezed flow parameter.
- The velocity profile shows opposite behavior for the Jeffrey model parameter and Deborah number.
- The velocity profile depicts an upsurging manner for magnetic parameter.
- Enhancement in fluid temperature is observed due to heat generation/absorption coefficient.
- The concentration of liquid drops with the enhancement of both thermophoretic and chemical reaction parameters.
- A decreasing behavior of the wall drag coefficient for the Jeffrey model parameter and an increasing behavior of the wall drag coefficient for Deborah number is observed.
- The Nusselt number increases as the squeezed flow parameter enhances and decreases for increment in heat generation coefficient.
- The Sherwood number exhibits an increasing phenomenon for both thermophoretic and chemical reaction parameters.

Acknowledgments

The authors extend their appreciation to University Higher Education Fund for funding this research work under Research Support Program for Central labs at King Khalid University through the project number CL/CO/A/1.

Data availability statement

No data created during this investigation. The data that support the findings of this study are available upon reasonable request from the authors.

Authors' contribution

Sajeel Mazhar: Writing—original draft. Muhammad Ramzan: Supervision, Conceptualization. Ahmed S. Sowayan: Methodology. C Ahamed Saleel: Formal analysis. Abdulkafi Mohammed Saeed: Investigation. Seifedine Kadry: Visualization. Mohammed El-Meligy: Validation.

Conflict of interest statement

Authors declare no conflict of interest.

ORCID iDs

Muhammad Ramzan https://orcid.org/0000-0002-9523-5800
C Ahamed Saleel https://orcid.org/0000-0003-3705-4371
Abdulkafi Mohammed Saeed https://orcid.org/0000-0001-9560-105X
Seifedine Kadry https://orcid.org/0000-0002-1939-4842
Mohammed A El-Meligy https://orcid.org/0000-0001-7967-4259

References

[1] Fetecau C, Mahmood A and Jamil M 2010 Exact solutions for the flow of a viscoelastic fluid induced by a circular cylinder subject to a time dependent shear stress *Commun. Nonlinear Sci. Numer. Simul.* **15** 3931–8
[2] Malik M Y, Hussain A and Nadeem S 2013 Boundary layer flow of an eyring-powell model fluid due to a stretching cylinder with variable viscosity *Scientia Iranica* **20** 313–21
[3] Hatami M and Ganji D D 2013 Heat transfer and flow analysis for SA-TiO_2 non-Newtonian nanofluid passing through the porous media between two coaxial cylinders *J. Mol. Liq.* **188** 155–61
[4] Ellahi R and Riaz A 2010 Analytical solutions for MHD flow in a third-grade fluid with variable viscosity *Math. Comput. Modell.* **52** 1783–93
[5] Nadeem S, Zaheer S and Fang T 2011 Effects of thermal radiation on the boundary layer flow of a Jeffrey fluid over an exponentially stretching surface *Numer. Algorithms* **57** 187–205
[6] Ahmad K and Ishak A 2016 MHD flow and heat transfer of a Jeffrey fluid over a stretching sheet with viscous dissipation *Malaysian journal of mathematical sciences* **10** 311–23
[7] Turkyilmazoglu M and Pop I 2013 Exact analytical solutions for the flow and heat transfer near the stagnation point on a stretching/shrinking sheet in a Jeffrey fluid *Int. J. Heat Mass Transfer* **57** 82–8
[8] Qasim M 2013 Heat and mass transfer in a Jeffrey fluid over a stretching sheet with heat source/sink *Alexandria Engineering Journal* **52** 571–5
[9] Bhatti M M and Abbas M A 2016 Simultaneous effects of slip and MHD on peristaltic blood flow of Jeffrey fluid model through a porous medium *Alexandria Engineering Journal* **55** 1017–23
[10] Kothandapani M and Srinivas S 2008 Peristaltic transport of a Jeffrey fluid under the effect of magnetic field in an asymmetric channel *Int. J. Non Linear Mech.* **43** 915–24
[11] Narayana P S and Babu D H 2016 Numerical study of MHD heat and mass transfer of a Jeffrey fluid over a stretching sheet with chemical reaction and thermal radiation *J. Taiwan Inst. Chem. Eng.* **59** 18–25
[12] Hayat T and Mustafa M 2010 Influence of thermal radiation on the unsteady mixed convection flow of a Jeffrey fluid over a stretching sheet *Z. Naturforsch.* A **65** 711–9
[13] Ramesh K and Joshi V 2019 Numerical solutions for unsteady flows of a magnetohydrodynamic Jeffrey fluid between parallel plates through a porous medium *Int. J. Comput. Methods Eng. Sci. Mech.* **20** 1–13
[14] Nadeem S, Akhtar S, Almutairi S, Ghazwani H A and Elkhatib S E 2022 Physical survey of thermally heated non-newtonian jeffrey fluid in a ciliated conduit having heated compressing and expanding walls *Applied Sciences* **12** 5065
[15] Nadeem S, Akhtar S, Akkurt N, Saleem A, Almutairi S and Ghazwani H A 2023 Physiological peristaltic flow of Jeffrey fluid inside an elliptic cross section with heat and mass transfer: exact solutions through polynomial solution technique. ZAMM-Journal of Applied Mathematics and Mechanics/Zeitschrift für *Angewandte Mathematik und Mechanik* **103** e202100383
[16] Stefan M J 1874 Versuchüber die scheinbare adhesion, SitzungsberSächsAkadWissWein *Math-Nat Wiss Kl* **69** 713–21
[17] Bhattacharyya S and Pal A 1997 Unsteady MHD squeezing flow between two parallel rotating discs *Mech. Res. Commun.* **24** 615–23
[18] Khan H, Qayyum M, Khan O and Ali M 2016 Unsteady squeezing flow of Casson fluid with magnetohydrodynamic effect and passing through porous medium *Mathematical Problems in Engineering* **2016**
[19] Salahuddin T, Malik M Y, Hussain A, Bilal S, Awais M and Khan I 2017 MHD squeezed flow of Carreau-Yasuda fluid over a sensor surface *Alexandria Engineering Journal* **56** 27–34
[20] Shankar U and Naduvinamani N B 2019 Magnetized squeezed flow of time-dependent Prandtl-Eyring fluid past a sensor surface *Heat Transfer—Asian Research* **48** 2237–61
[21] Khan M, Malik M Y, Salahuddin T and Khan I 2016 Heat transfer squeezed flow of Carreau fluid over a sensor surface with variable thermal conductivity: a numerical study *Results in physics* **6** 940–5
[22] Muhammad T, Hayat T, Alsaedi A and Qayyum A 2017 Hydromagnetic unsteady squeezing flow of Jeffrey fluid between two parallel plates *Chin. J. Phys.* **55** 1511–22
[23] Muhammed R K, Basha H, Reddy G J, Shankar U and Bég O A 2022 Influence of variable thermal conductivity and dissipation on magnetic Carreau fluid flow along a micro-cantilever sensor in a squeezing regime *Waves Random Complex Medium* 1–30

[24] Alharbi K A M, Shahmir N, Ramzan M, Almusawa M Y and Kadry S 2024 Bioconvective radiative unsteady Casson nanofluid flow across two concentric stretching cylinders with variable viscosity and variable thermal conductivity *Numerical Heat Transfer, Part A: Applications* **85** 1653–70
[25] Atif S M, Hussain S and Sagheer M 2019 Effect of thermal radiation and variable thermal conductivity on magnetohydrodynamics squeezed flow of Carreau fluid over a sensor surface *Journal of Nanofluids* **8** 806–16
[26] Kumar K G, Gireesha B J, Krishanamurthy M R and Rudraswamy N G 2017 An unsteady squeezed flow of a tangent hyperbolic fluid over a sensor surface in the presence of variable thermal conductivity *Results in physics* **7** 3031–6
[27] Hamad M A A, AbdEl-Gaied S M and Khan W A 2013 Thermal jump effects on boundary layer flow of a Jeffrey fluid near the stagnation point on a stretching/shrinking sheet with variable thermal conductivity *Journal of Fluids* **2013**
[28] Ramesh G K, Madhukesh J K, Shehzad S A and Rauf A 2024 Ternary nanofluid with heat source/sink and porous medium effects in stretchable convergent/divergent channel *Proc. Inst. Mech. Eng. Part E J. Process Mech. Eng.* **238** 134–43
[29] Madhukesh J K, Mansir I B, Prasannakumara B C, Khan M I, Alharbi K A M, Abdelrahman A and El-Sayed Ahmed A 2022 Combined impact of Marangoni convection and thermophoretic particle deposition on chemically reactive transport of nanofluid flow over a stretching surface *Nanotechnology Reviews* **11** 2202–14
[30] Khan M and Hamid A 2017 Influence of non-linear thermal radiation on 2D unsteady flow of a Williamson fluid with heat source/sink *Results in Physics* **7** 3968–75
[31] Goren S L 1977 Thermophoresis of aerosol particles in the laminar boundary layer on a flat plate *J. Colloid Interface Sci.* **61** 77–85
[32] Chiou M C 1998 Particle deposition from natural convection boundary layer flow onto an isothermal vertical cylinder *Acta Mech.* **129** 163–76
[33] Doh D H and Muthtamilselvan M 2017 Thermophoretic particle deposition on magnetohydrodynamic flow of micropolar fluid due to a rotating disk *Int. J. Mech. Sci.* **130** 350–9
[34] Hafeez A, Khan M and Ahmed J 2021 Oldroyd-B fluid flow over a rotating disk subject to Soret–Dufour effects and thermophoresis particle deposition *Proc. Inst. Mech. Eng. Part C J. Mech. Eng. Sci.* **235** 2408–15
[35] Chen S B, Shahmir N, Ramzan M, Sun Y L, Aly A A and Malik M Y 2021 Thermophoretic particle deposition in the flow of dual stratified Casson fluid with magnetic dipole and generalized Fourier's and Fick's laws *Case Studies in Thermal Engineering* **26** 101186
[36] Kumar R N, Punith Gowda R J, Prasanna G D, Prasannakumara B C, Nisar K S and Jamshed W 2021 Comprehensive study of thermophoretic diffusion deposition velocity effect on heat and mass transfer of ferromagnetic fluid flow along a stretching cylinder *Proc. Inst. Mech. Eng. Part E J. Process Mech. Eng.* **235** 1479–89
[37] Kumar R N, Gowda R P, Madhukesh J K, Prasannakumara B C and Ramesh G K 2021 Impact of thermophoretic particle deposition on heat and mass transfer across the dynamics of Casson fluid flow over a moving thin needle *Phys. Scr.* **96** 075210
[38] Kumar R N, Jyothi A M, Alhumade H, Gowda R P, Alam M M, Ahmad I and Prasannakumara B C 2021 Impact of magnetic dipole on thermophoretic particle deposition in the flow of Maxwell fluid over a stretching sheet *J. Mol. Liq.* **334** 116494
[39] Ramzan M, Gul H, Ghazwani H A S, Nisar K S, Abbas M, Saleel C V A and Kadry S 2023 Influence of variable thermal conductivity and diffusion coefficients in the flow of Jeffrey fluid past a lubricated surface with homogeneous-heterogeneous reactions: a finite-difference approximations *Numerical Heat Transfer, Part A: Applications* **84** 1107–23
[40] Basha H, Nandeppanavar M M and Reddy G J 2024 Dissipative Lorentz force influence on mass flow over a micro-cantilever sensor sheet under magnetic Ohmic heating. ZAMM-Journal of applied mathematics and mechanics/zeitschrift für *Angewandte Mathematik und Mechanik* **104** e202300055
[41] Azam M, Xu T and Khan M 2020 Numerical simulation for variable thermal properties and heat source/sink in flow of Cross nanofluid over a moving cylinder *Int. Commun. Heat Mass Transfer* **118** 104832
[42] Salahuddin T, Mahmood Z, Khan M and Awais M 2022 A permeable squeezed flow analysis of Maxwell fluid near a sensor surface with radiation and chemical reaction *Chem. Phys.* **562** 111627
[43] Ramesh G K, Madhukesh J K, Shah N A and Yook S J 2023 Flow of hybrid CNTs past a rotating sphere subjected to thermal radiation and thermophoretic particle deposition *Alexandria Engineering Journal* **64** 969–79
[44] Alharbi K A M, Ramzan M, Shahmir N, Ghazwani H A S, Elmasry Y, Eldin S M and Bilal M 2023 Comparative appraisal of mono and hybrid nanofluid flows comprising carbon nanotubes over a three-dimensional surface impacted by Cattaneo–Christov heat flux. *Sci. Rep.* **13** 7964
[45] Rammoorthi R and Mohanavel D 2023 Numerical simulation of an electromagnetic squeezing hybrid nanofluid flow through permeable plates with sensor monitoring system *Phys. Fluids* **35** 093615